

## **Supplementary Materials**

**Amine-functionalized porous aromatic frameworks for efficient adsorption of hazardous organic micropollutants in water**

**Ayesha Javaid<sup>1</sup>, Talal Ahmad<sup>1</sup>, Changyan Zhu<sup>1</sup>, Hengtao Lei<sup>1</sup>, Noman Ali Shah<sup>2</sup>, Zilong Dou<sup>1</sup>, Yongyue Ding<sup>1</sup>, Yunxuan Li<sup>1</sup>, Yuyang Tian<sup>1,\*</sup>**

<sup>1</sup>Key Laboratory of Polyoxometalate and Reticular Material Chemistry of Ministry of Education, Faculty of Chemistry, Northeast Normal University, Changchun 130024, Jilin, China.

<sup>2</sup>State Environmental Protection Key Laboratory of Wetland Ecology and Vegetation Restoration, School of Environment, Northeast Normal University, Changchun 130117, Jilin, China.

**\*Correspondence to:** Prof. Yuyang Tian, Key Laboratory of Polyoxometalate and Reticular Material Chemistry of Ministry of Education, Faculty of Chemistry, Northeast Normal University, Changchun 130024, Jilin, China. Email: tianyy100@nenu.edu.cn

## Table of Contents

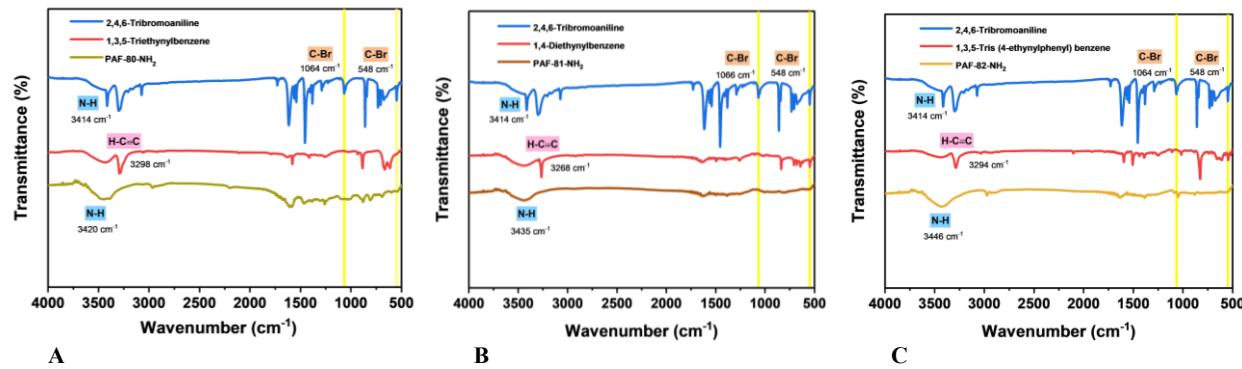
Supplementary Table 1.....	3
Supplementary Section 1.....	3
Supplementary Figure 1.....	4
Supplementary Figure 2.....	4
Supplementary Figure 3.....	5
Supplementary Figure 4.....	5
Supplementary Figure 5.....	6
Supplementary Figure 6.....	6
Supplementary Figure 7.....	7
Supplementary Table 2.....	8
Supplementary Figure 8.....	9
Supplementary Figure 9.....	10
Supplementary Figure 10.....	11
Supplementary Figure 11.....	12
Supplementary Figure 12.....	13
Supplementary Figure 13.....	14
Supplementary Figure 14.....	15
Supplementary Figure 15.....	15
Supplementary Table 3.....	15
Supplementary Figure 16.....	16
Supplementary Table 4.....	17
Supplementary Figure 17.....	18
References.....	19

**Supplementary Table 1. Mole ratios of building units and catalysts for amine-functionalized PAF materials**

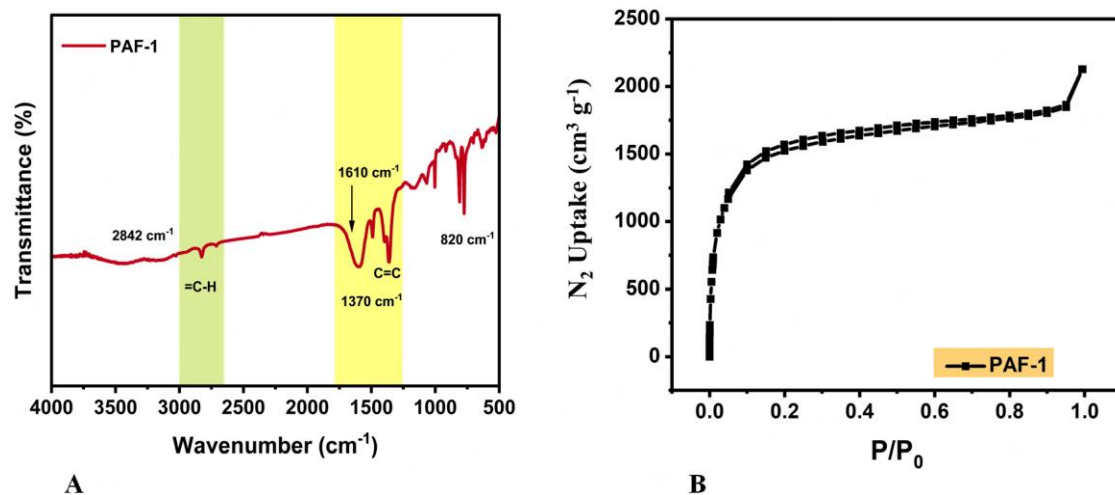
Materials	2,4,6-tribromo aniline	Building units	Tetrakis(triphenyl-phosphine)palladium	CuI	Triethylamine /DMF V: V	Yield (%)
PAF-80-NH <sub>2</sub>	0.6 mmole	0.6 mmole	457 mg	15mg	15 ml:15 ml	91
PAF-81-NH <sub>2</sub>	0.6 mmole	0.9 mmole	457 mg	15mg	15 ml:15 ml	89
PAF-82-NH <sub>2</sub>	0.6 mmole	0.6 mmole	457 mg	15mg	15 ml:15 ml	96

**Supplementary Section 1. Synthetic procedure of PAF-1**

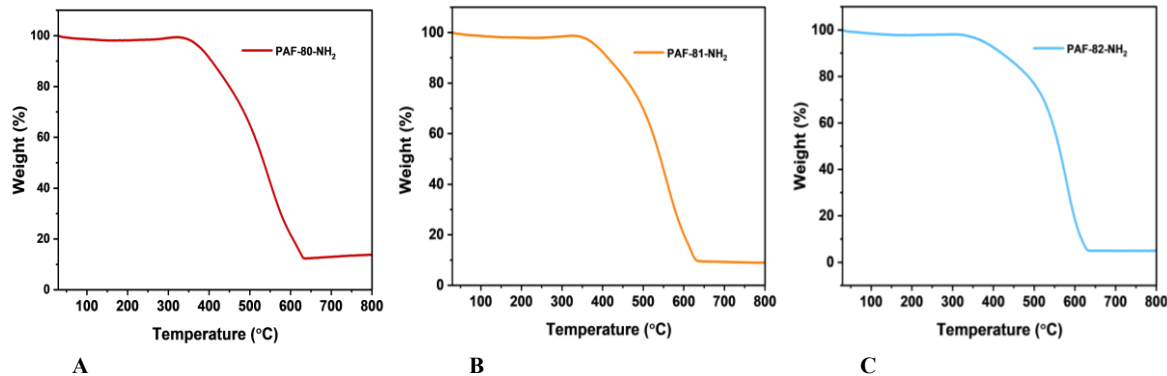
PAF-1 was synthesized following the procedure in already reported literature<sup>[1]</sup>. For its synthesis, 1,5-cyclooctadiene (cod, 1.05 mL, 8.32 mmol) was introduced into the solution of the catalyst as bis(1,5-cyclooctadiene) nickel(0) {[Ni(cod)<sub>2</sub>]}) (2.25 g, 8.18 mmol), and 2,2'-bipyridyl (1.28 g, 8.18 mmol) in extra dry DMF (50 mL). Then, this round bottom flask was left at 80 °C for 1 h for activation of catalyst. On the other hand, monomer tetrakis(4-bromophenyl) methane (1 g, 1.57 mmol) was completely dispersed in the same solvent, extra dry DMF (70 mL), then added to purple catalyst solution at 80 °C. This resultant mixture was stirred overnight at the same temperature to get a deep purple suspension. Concentrated HCl was added to the mixture after cooling it to room temperature to stop the reaction. Consequently, three washings with CHCl<sub>3</sub>, THF, and H<sub>2</sub>O were carried out after filtration. After Soxhlet extraction in THF and vacuum, drying, off-white colored powder was obtained as PAF-1.



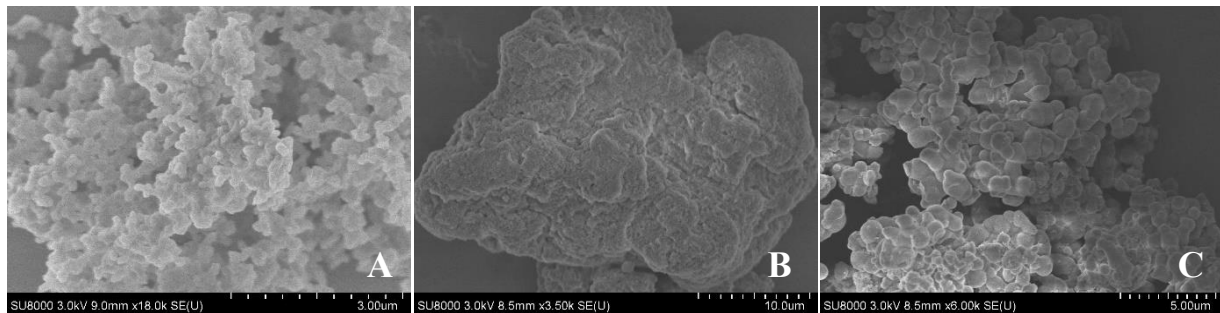
**Supplementary Figure 1.** FTIR spectra of synthesized amine-functionalized PAFs: (A) FTIR spectra of PAF-80-NH<sub>2</sub>; (B) FTIR spectra of PAF-81-NH<sub>2</sub>; (C) FTIR spectra of PAF-82-NH<sub>2</sub>.



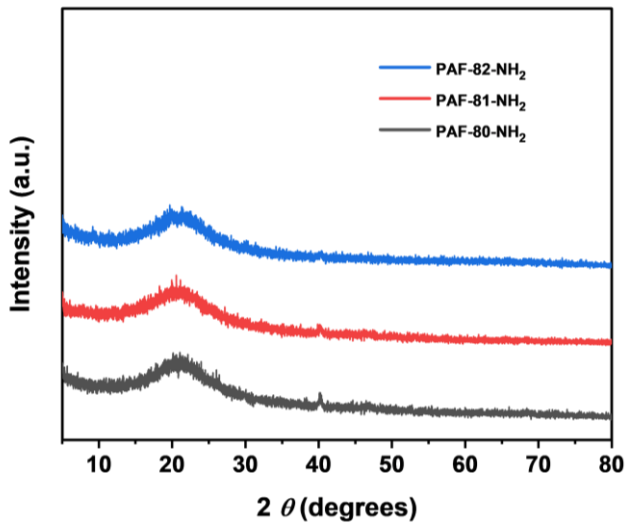
**Supplementary Figure 2.** Characterization of PAF-1: (A) FTIR of PAF-1; (B) N<sub>2</sub> isotherm of PAF-1.



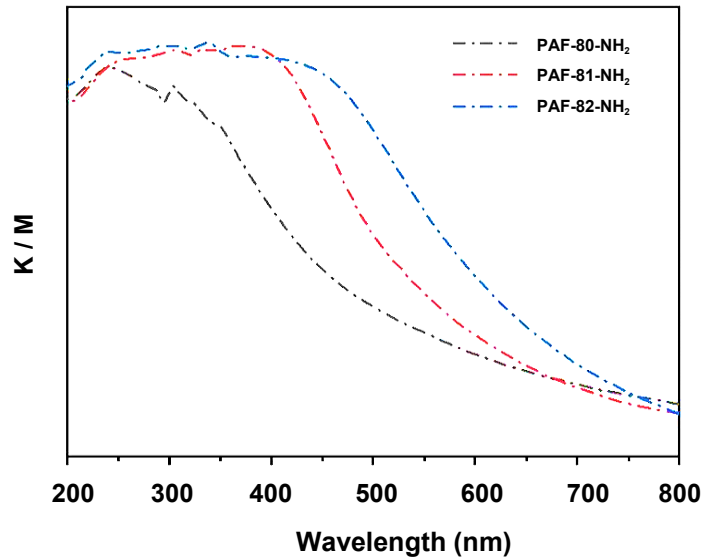
**Supplementary Figure 3.** TGA curves of synthesized amine-functionalized PAFs under air at 10 °C/min: (A) TGA curve of PAF-80-NH<sub>2</sub>; (B) TGA curve of PAF-81-NH<sub>2</sub>; (C) TGA curve of PAF-82-NH<sub>2</sub>.



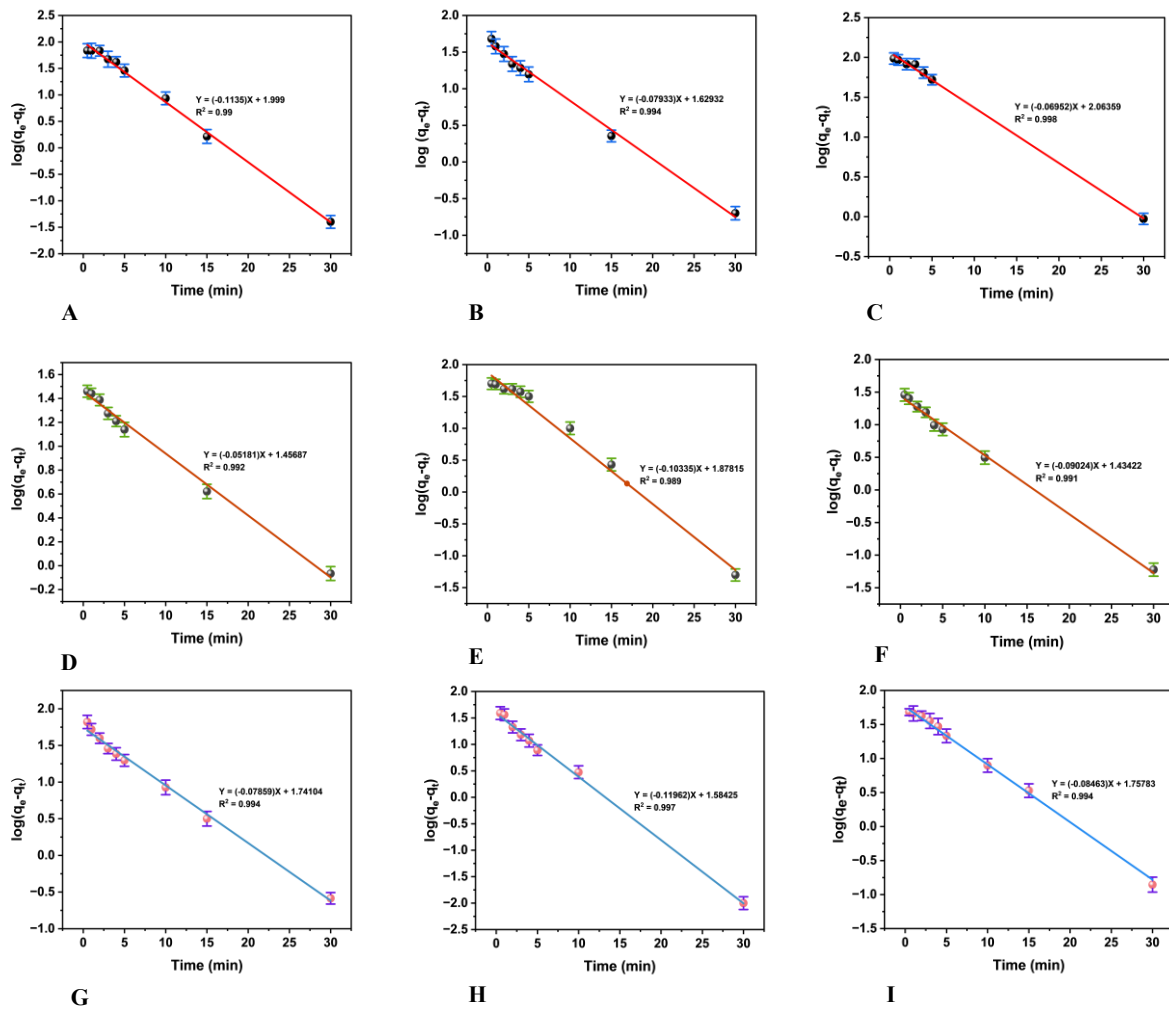
**Supplementary Figure 4.** SEM images of synthesized amine-functionalized PAFs: (A) SEM image of PAF-80-NH<sub>2</sub>; (B) SEM image of PAF-81-NH<sub>2</sub>; (C) SEM image of PAF-82-NH<sub>2</sub>.



**Supplementary Figure 5.** PXRD pattern of PAF-80-NH<sub>2</sub> (**black**), PAF-81-NH<sub>2</sub> (**red**), and PAF-82-NH<sub>2</sub> (**blue**).



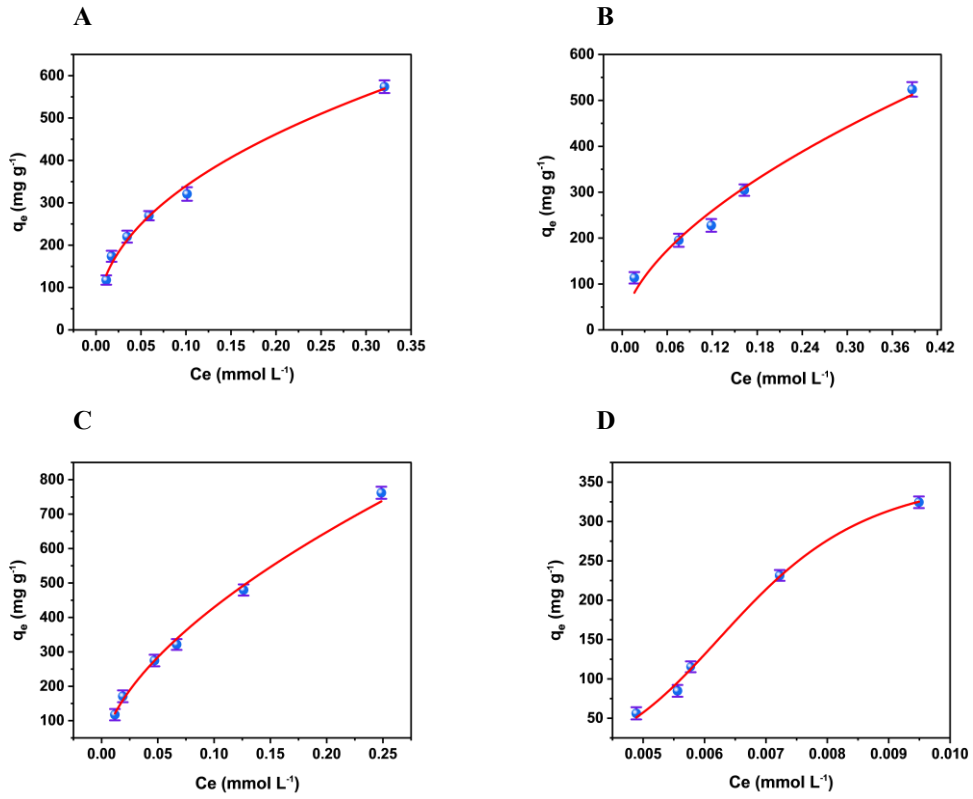
**Supplementary Figure 6.** UV-visible reflectance spectra of PAF-80-NH<sub>2</sub> (**black**), PAF-82-NH<sub>2</sub> (**red**) and PAF-81-NH<sub>2</sub> (**blue**).



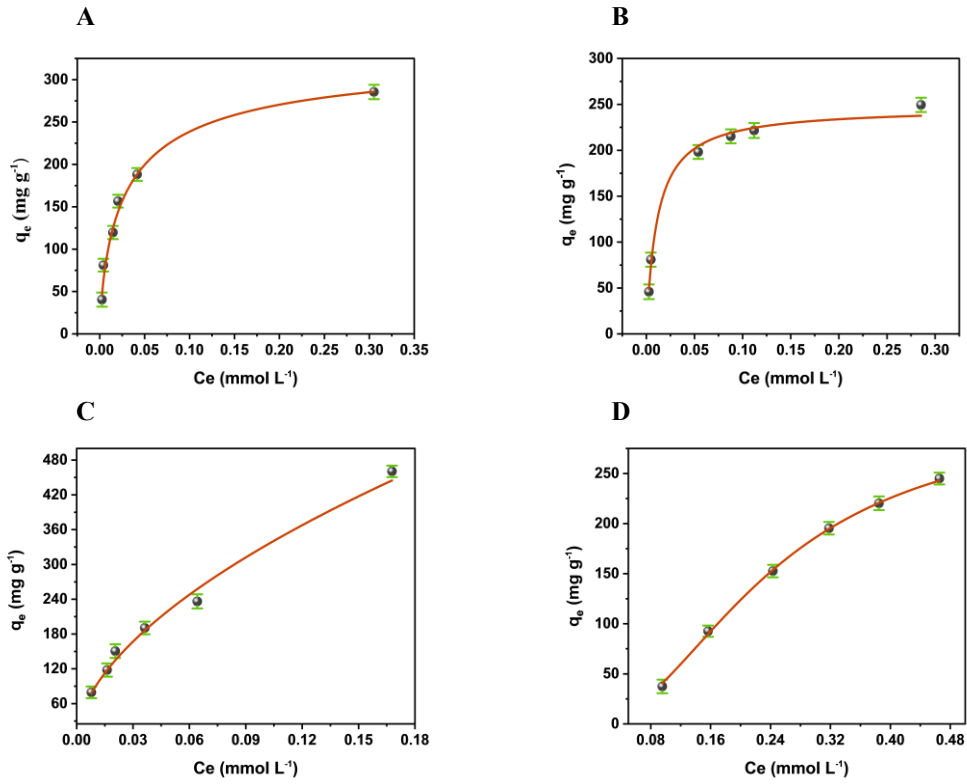
**Supplementary Figure 7.** Linear fitting curves of Pseudo-first-order kinetic data: (A) BPA adsorption by PAF-80-NH<sub>2</sub>; (B) BPA adsorption by PAF-81-NH<sub>2</sub>; (C) BPA adsorption by PAF-82-NH<sub>2</sub>; (D) 2-NO adsorption by PAF-80-NH<sub>2</sub>; (E) 2-NO adsorption by PAF-81-NH<sub>2</sub>; (F) 2-NO adsorption by PAF-82-NH<sub>2</sub>; (G) PCMX adsorption by PAF-80-NH<sub>2</sub>; (H) PCMX adsorption by PAF-81-NH<sub>2</sub>; (I) PCMX adsorption by PAF-82-NH<sub>2</sub>.

**Supplementary Table 2. Fitting parameters of pseudo-first-order kinetics and pollutant uptake rates by amine-functionalized PAF materials.**

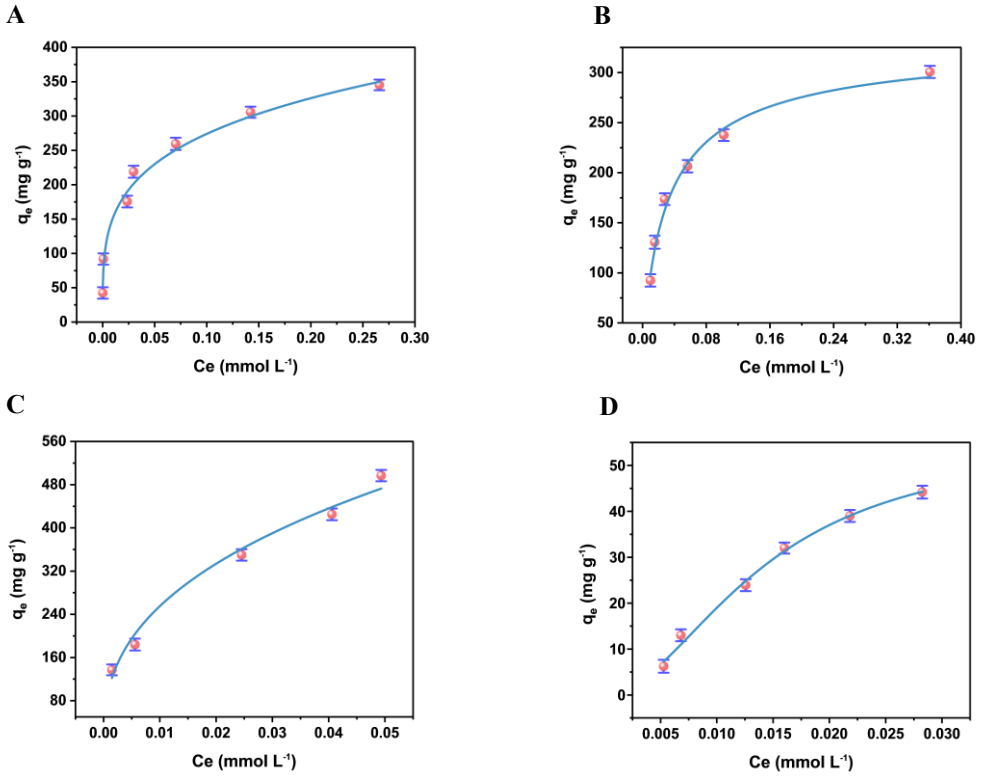
Sorbent	BPA			2-NO			PCMX		
	K ( $\text{g}\cdot\text{mg}^{-1}\cdot\text{min}^{-1}$ )	R <sup>2</sup>	t <sub>eq</sub> (min)	K ( $\text{g}\cdot\text{mg}^{-1}\cdot\text{min}^{-1}$ )	R <sup>2</sup>	t <sub>eq</sub> (min)	K ( $\text{g}\cdot\text{mg}^{-1}\cdot\text{min}^{-1}$ )	R <sup>2</sup>	t <sub>eq</sub> (min)
PAF-80-NH <sub>2</sub>	0.2614	0.990	20	0.1193	0.994	20	0.1810	0.998	25
PAF-81-NH <sub>2</sub>	0.1827	0.992	30	0.2380	0.989	25	0.2755	0.991	30
PAF-82-NH <sub>2</sub>	0.1601	0.99	15	0.2078	0.99	20	0.19	0.994	10



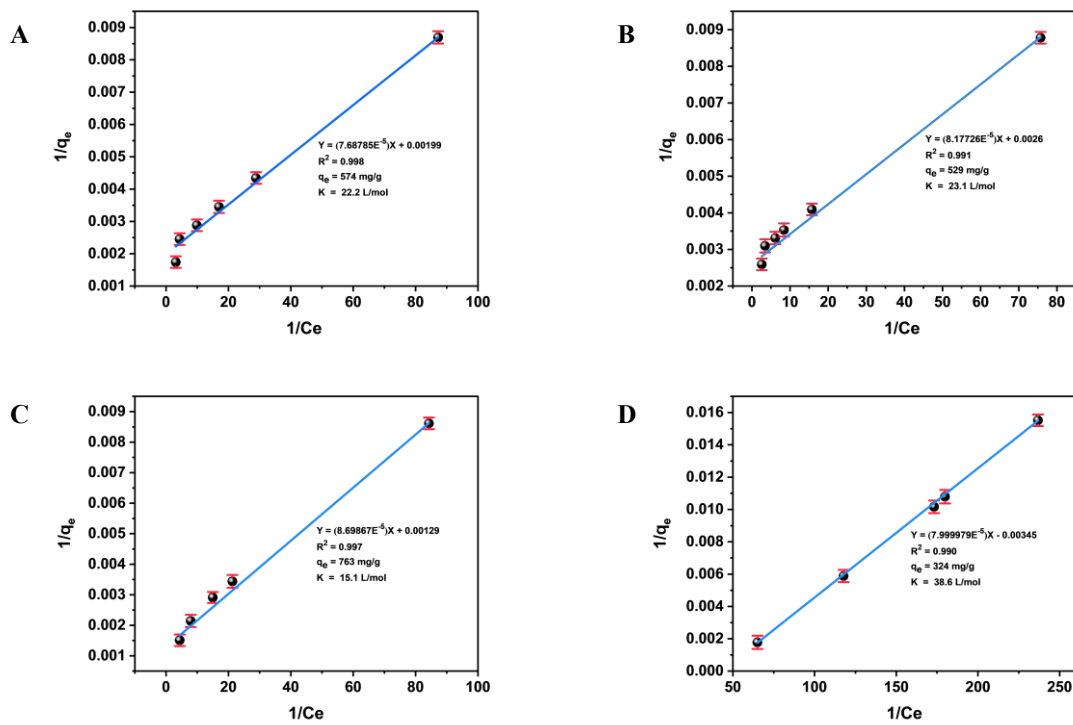
**Supplementary Figure 8.** Langmuir adsorption isotherms: (A) BPA adsorption onto PAF-80-NH<sub>2</sub>; (B) BPA adsorption onto PAF-81-NH<sub>2</sub>; (C) BPA adsorption onto PAF-82-NH<sub>2</sub>; (D) BPA adsorption onto PAF-1.



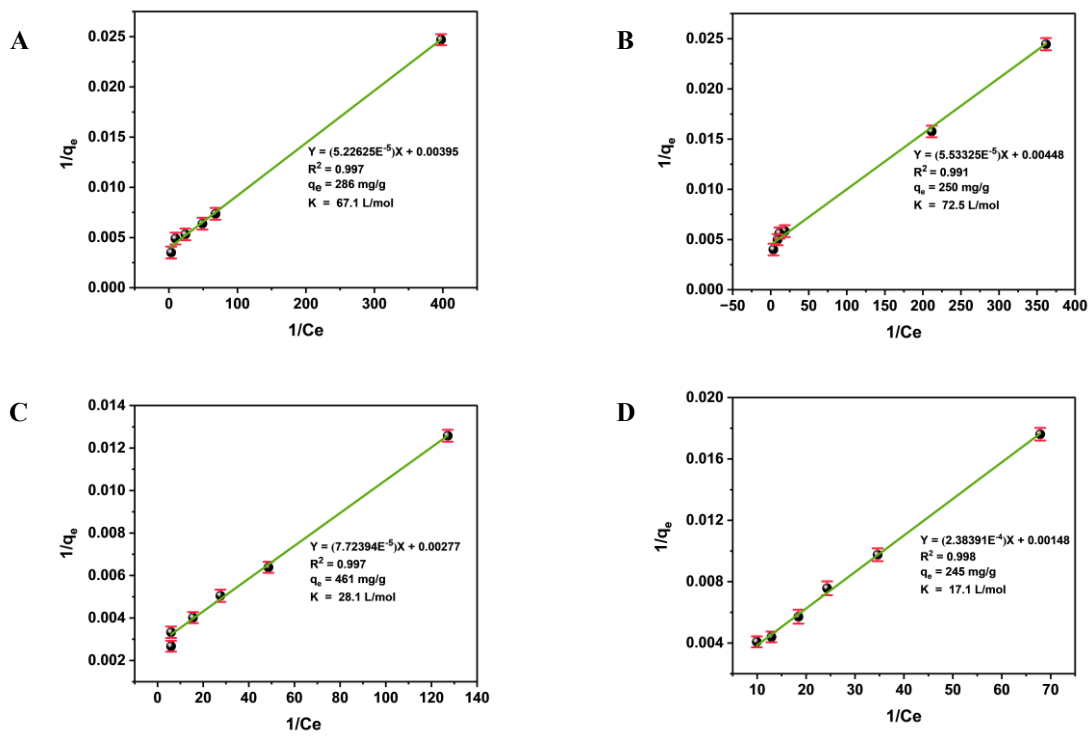
**Supplementary Figure 9.** Langmuir adsorption isotherms. (A) 2-NO adsorption onto PAF-80-NH<sub>2</sub>; (B) 2-NO adsorption onto PAF-81-NH<sub>2</sub>; (C) 2-NO adsorption onto PAF-82-NH<sub>2</sub>; (D) 2-NO adsorption onto PAF-1.



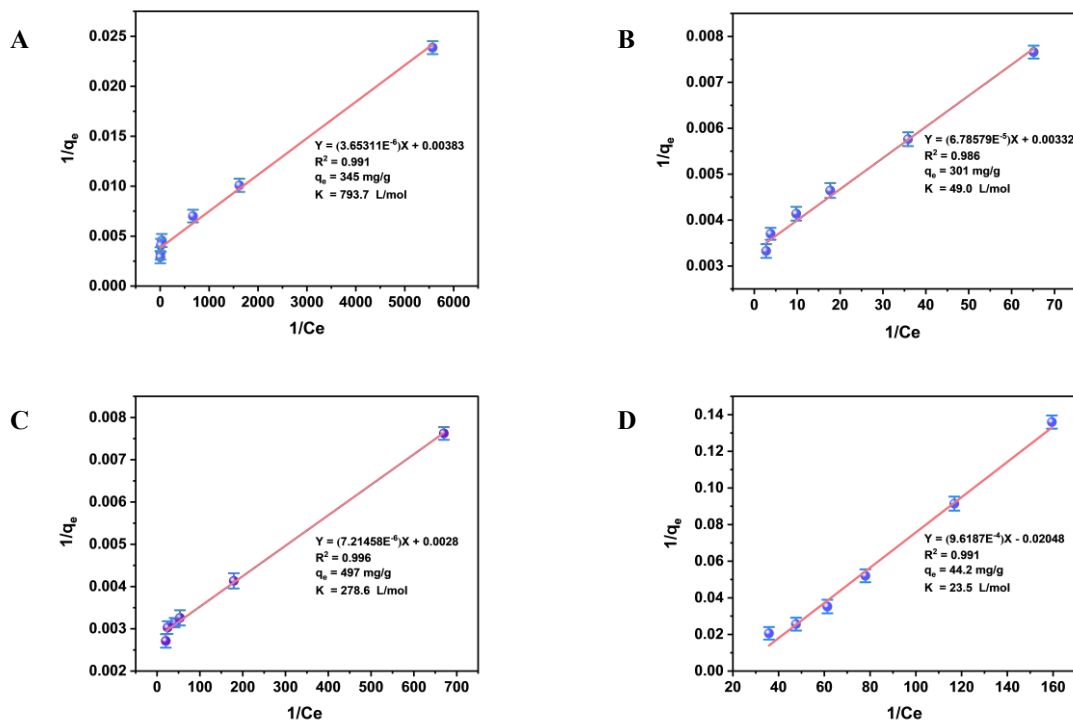
**Supplementary Figure 10.** Langmuir adsorption isotherms: (A) PCMx adsorption onto PAF-80-NH<sub>2</sub>; (B) PCMx adsorption onto PAF-81-NH<sub>2</sub>; (C) PCMx adsorption onto PAF-82-NH<sub>2</sub>; (D) PCMx adsorption onto PAF-1.



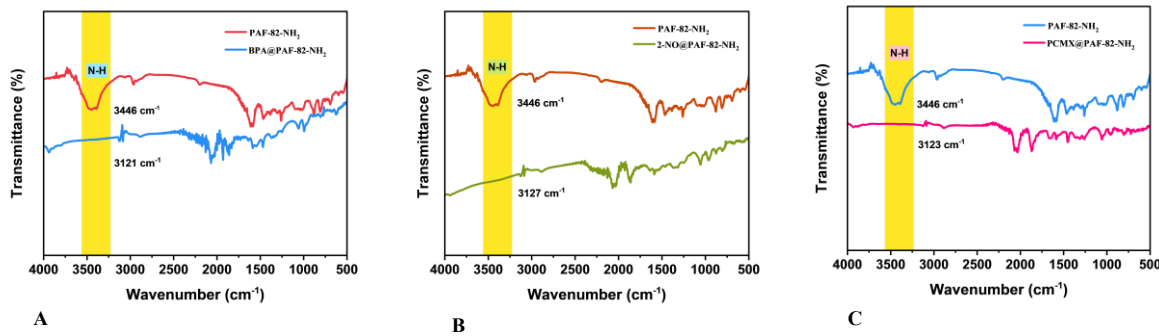
**Supplementary Figure 31.** Langmuir linear plots: (A) BPA adsorption onto PAF-80-NH<sub>2</sub>; (B) BPA adsorption onto PAF-81-NH<sub>2</sub>; (C) BPA adsorption onto PAF-82-NH<sub>2</sub>; (D) BPA adsorption onto PAF-1.



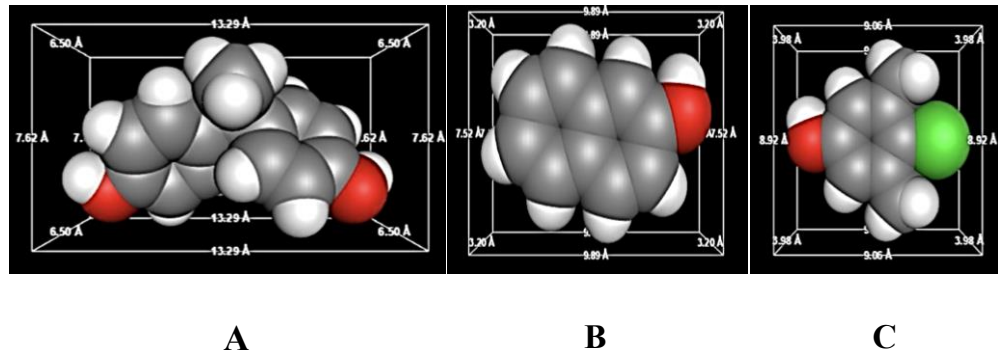
**Supplementary Figure 42.** Langmuir linear plots: (A) 2-NO adsorption onto PAF-80-NH<sub>2</sub>; (B) 2-NO adsorption onto PAF-81-NH<sub>2</sub>; (C) 2-NO adsorption onto PAF-82-NH<sub>2</sub>; (D) 2-NO adsorption onto PAF-1.



**Supplementary Figure 13.** Langmuir linear plots: (A) PCMx adsorption onto PAF-80-NH<sub>2</sub>; (B) PCMx adsorption onto PAF-81-NH<sub>2</sub>; (C) PCMx adsorption onto PAF-82-NH<sub>2</sub>; (D) PCMx adsorption onto PAF-1.



**Supplementary Figure 5.** FTIR spectra of Amine-functionalized PAFs before and after adsorption of OMP: (A) BPA adsorption onto PAF-82-NH<sub>2</sub>; (B) 2-NO adsorption onto PAF-82-NH<sub>2</sub>; (C) PCMX adsorption onto PAF-82-NH<sub>2</sub>.

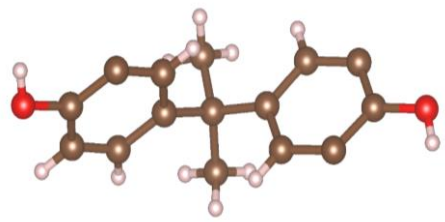


**Supplementary Figure 6.** Molecular dimensions of OMP: (A) BPA; (B) 2-NO; (C) PCMX.

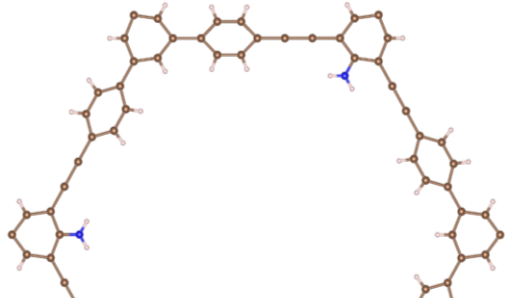
**Supplementary Table 3. Comparison of molecular dimensions of OMP with PAF-82-NH<sub>2</sub> pore size.**

Model OMPs	OMP dimensions (Å)	Pore size (Å) (PAF-82-NH <sub>2</sub> )	Accessibility
BPA	13.29 × 7.62 × 6.50	13.79	Accessible
2-NO	9.89 × 7.52 × 3.20	13.79	Accessible
PCMX	9.06 × 8.92 × 3.98	13.79	Accessible

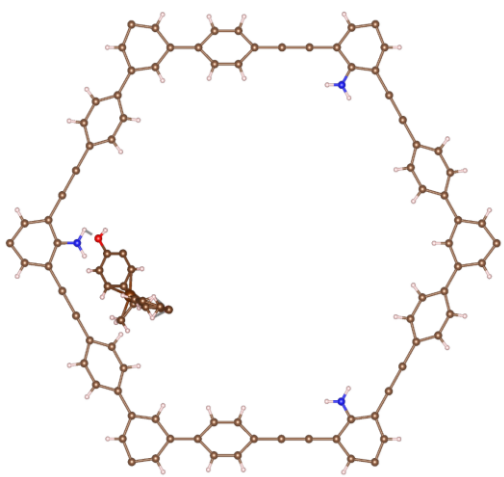
**A**



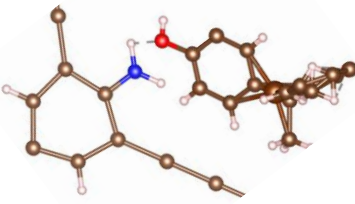
**B**



**C**



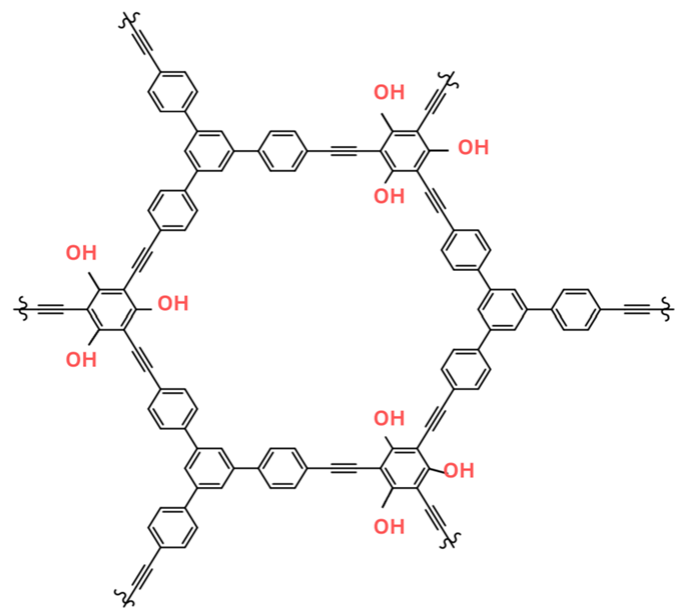
**D**



**Supplementary Figure 7.** Representation of optimized structures: (A) BPA; (B) PAF-82-NH<sub>2</sub>; (C) BPA adsorbed onto PAF-82-NH<sub>2</sub>; (D) Zoomed view of BPA adsorption onto PAF-82-NH<sub>2</sub>.

**Supplementary Table 4. Adsorption capacities ( $\text{mg}\cdot\text{g}^{-1}$ ) of some recently reported adsorbents**

Adsorbents	Pollutants	Adsorption Capacity (mg/g)	References
PAF-82	BPA	689	[1]
lignin-based activated carbon (KLP)	BPA	220	[2]
hierarchically porous biochar (HBC)	BPA	246.13	[3]
Graphene oxide diethylenetriamine GO-DEA	BPA	334.4	[4]
Metal-organic-framework-derived carbon (MDC-800)	BPA	493	[5]
Al-MOF-NH <sub>2</sub>	BPA	227.78	[5]
azine-linked COF	BPA	61.3	[5]
PAF-82-NH <sub>2</sub>	BPA	763	This work
ZIF@wool	2-NO	371.2-391.1	[6]
PAF-82	2-NO	431	[1]
Biochar (200-1)	2-NO	230.45	[7]
PAF-82-NH <sub>2</sub>	2-NO	461	This work
β-CDP	PCMX	144	[8]
PAF-82	PCMX	480	[1]
MONTs-pNIAPM sponge	PCMX	184	[9]
Co-NPC-800	PCMX	39	[10]
PAF-82-NH <sub>2</sub>	PCMX	497	This work



**Supplementary Figure 8.** Structure of hydroxyl-functionalized PAF-82<sup>[1]</sup>.

## REFERENCES

1. Mo, C.; Faheem, M.; Aziz, S.; et al. Hydroxyl porous aromatic frameworks for efficient adsorption of organic micropollutants in water. *RSC. Adv.* **2020**, *10*, 26335-41. [DOI](#) [PubMed](#)
2. Hernández-Abreu, A. B.; Álvarez-Torrellas, S.; Rocha, R. P.; et al. Effective adsorption of the endocrine disruptor compound Bisphenol a from water on surface-modified carbon materials. *Appl. Surf. Sci.* **2021**, *552*, 149513. [DOI](#)
3. Shi, W.; Wang, H.; Yan, J.; Shan, L.; Quan, G.; Pan, X.; et al. Wheat straw derived biochar with hierarchically porous structure for bisphenol A removal: preparation, characterization, and adsorption properties. *Sep. Purif. Technol.* **2022**, *289*, 120796. [DOI](#)
4. Al-Qadri, A. A. Q.; Drmosh, Q. A.; Onaizi, S. A. Enhancement of bisphenol a removal from wastewater via the covalent functionalization of graphene oxide with short amine molecules. *CSCE* **2022**, *6*, 100233. [DOI](#)
5. Cheng, F.; Wang, J. Removal of Bisphenol a from wastewater by adsorption and membrane separation: performances and mechanisms. *Chem. Eng. J.* **2024**, *484*, 149414. [DOI](#)
6. Abdelhameed, R. M.; Emam, H. E. Design of ZIF(Co & Zn)@wool composite for efficient removal of pharmaceutical intermediate from wastewater. *J. Colloid Interface Sci.* **2019**, *552*, 494-505. [DOI](#) [PubMed](#)
7. Temur Ergan, B.; Aydin, E. S.; Gengec, E. The effect of various thermochemical methods on the production of biochar and removal of 2-naphthol orange from wastewater. *J Chem Technol Biot* **2024**, *99*, 81-91. [DOI](#)
8. Zhou, Y.; Cheng, G.; Chen, K.; Lu, J.; Lei, J.; Pu, S. Adsorptive removal of bisphenol A, chloroxylenol, and carbamazepine from water using a novel β-cyclodextrin polymer. *Ecotoxicol. Environ. Saf.* **2019**, *170*, 278-285. [DOI](#)
9. Li, Q.; Zhu, S.; Hao, G.; Hu, Y.; Wu, F.; Jiang, W. Fabrication of thermoresponsive metal-organic nanotube sponge and its application on the adsorption of endocrine-disrupting compounds and pharmaceuticals/personal care products: experiment and molecular simulation study. *Environ. Pollut.* **2021**, *273*, 116466. [DOI](#) [PubMed](#)
10. Li, Q.; Huang, L.; Zhu, P.; Zhong, M.; Xu, S. Rapid adsorption of Triclosan and P-Chloro-m-Xylenol by nitrogen-doped magnetic porous carbon. *Environ. Sci. Pollut. Res. Int.* **2023**, *30*, 1640-1655. [DOI](#) [PubMed](#)